

# Finite temperature thermodynamic properties of the spin-1 nematics in an applied magnetic field

Katsuhiro Tanaka<sup>1</sup> and Chisa Hotta<sup>1</sup>

<sup>1</sup>*Department of Basic Science, University of Tokyo, Meguro, Tokyo 153-8902, Japan*

(Dated: September 17, 2020)

We study numerically the thermodynamic properties of the spin nematic phases in a magnetic field in the spin-1 bilinear-biquadratic model. When the field is applied, the phase transition temperature once goes up and then decreases rapidly toward zero, which is detected by the peak-shift in the specific heat. The underlying mechanism of the reentrant behavior is the entropic effect. In a weak field the high temperature paramagnetic phase rapidly loses its entropy while the ferroquadrupolar nematic phase remains robust by modifying the shape of the ferroquadrupolar moment. This feature serves as a fingerprint of generic ferroquadrupolar phases, while it is not observed for the case of antiferroquadrupoles.

*Introduction.* Among symmetry broken phases in solids, those of higher order multipolar degrees of freedom are hard to study and have been often referred to as “hidden orders”. This is because their order parameters are not linearly coupled to external fields or forces, and thus are extremely difficult to characterize by the conventional experimental probes, as well known in heavy fermion examples like CeB<sub>6</sub> [1, 2], URu<sub>2</sub>Si<sub>2</sub> [3, 4]. Still, making use of the coupling between wave function and the crystal lattice distortion, the electronic quadrupolar orderings in CeB<sub>6</sub> is detected by the elasticity measurements [5]. The elasto-resistivity measurements are also performed for the clarification of the orbital nematics in iron pnictide [6].

In quantum magnets, the quadrupolar orderings of localized spins are often referred to as spin nematics. Unlike the true hidden orders, the quadrupolar spin moments are already well-defined in theories [7]. Nevertheless, the spin nematics are still “hidden” in the sense that they are often invisible to local magnetic probes like neutron scattering or magnetic resonances and only show featureless paramagnetic-like responses to static magnetic field. Efforts on measuring the dynamical quantities have been made [8–23], e.g, in the nuclear magnetic resonance [10–14, 16, 21] and inelastic neutron scattering [17, 19], or the electron spin resonance [20, 22], while experiments and theories are practically difficult to reconcile.

Spin nematics can resort to Landau’s approaches on second order phase transitions, where some anomalies are found in the magnetocaloric and in the ac magnetic susceptibility measurements [24–26]. In theories, finite temperature phase diagrams of spin-1 nematics at zero field are studied for the square lattice [27, 28] and the triangular lattice [29, 30] by the quantum Monte Carlo (QMC) simulation, and for the triangular lattice by the variational method [31]. However, the basic information on how the quadrupolar moments of spin-1 respond to a magnetic field and they modify the finite temperature properties remain unexplored.

In this paper, we examine this issue by applying the Monte Carlo simulations to the spin-1 bilinear-

biquadratic (BLBQ) model, a canonical model for spin nematics. A pure quantum quadrupole is represented by a director  $\mathbf{d}$ , a real vector pointing perpendicular to the fluctuating spin moments, which does not couple to a magnetic field. However, the imaginary component of  $\mathbf{d}$  relevant to the emergent dipole moment couples to the field, which modifies the shape of the quadrupole to those fluctuating in-plane [8]. Since this modification keeps the spin nematic state robust against the weak field, the transition temperature once slightly goes up and then starts to decrease at stronger field. The former behavior reminds us of the Pomeranchuk effect in <sup>3</sup>He [32] whose liquid and solid phases may roughly correspond to our nematic and paramagnetic phases, respectively. In fact, the paramagnetic phase rapidly loses its entropy with an applied field and gives way to the nematic phase, just like decreasing the pressure in <sup>3</sup>He will transform the solid to liquid by releasing the entropy. The reentrant effect is a general feature of the ferroquadrupolar nematic phase as it is observed also in a square lattice, whereas not in the antiferroquadrupolar phases.

*Spin-1 bilinear-biquadratic model.* We deal with the spin-1 BLBQ model on the triangular and square lattices in a magnetic field;

$$\mathcal{H} = \sum_{\langle i,j \rangle} \left[ J \hat{\mathbf{S}}_i \cdot \hat{\mathbf{S}}_j + K \left( \hat{\mathbf{S}}_i \cdot \hat{\mathbf{S}}_j \right)^2 \right] - h \sum_{i=1}^N \hat{S}_i^z, \quad (1)$$

where  $\hat{\mathbf{S}}_i$  is the spin-1 operator on site- $i$  with  $i = 1-N$ , and  $J$ ,  $K$ , and  $h$  denote the Heisenberg (bilinear) and the biquadratic (BQ) interactions, the magnetic field applied parallel to the  $z$ -axis, respectively. Hereafter,  $J$  and  $K$  are normalized as  $J^2 + K^2 = 1$ .

Semiclassical approaches using the variational method revealed that in the absence of a magnetic field, the ground state of Eq. (1) has a FQ order for  $K/J < \tan^{-1}(-2)$  with  $J > 0$ , or  $K < J \leq 0$  for the triangular lattice, and  $K < J < 0$  for the square lattice [8, 33, 34], which agree qualitatively well with those from the fully quantum approaches. When a magnetic field is applied along the  $z$ -axis, the FQ state acquires a small but finite magnetic moment along the  $z$ -axis while retains its

quadrupolar moment in the  $xy$ -plane, but finally turns into a fully polarized magnetic phase at  $h = z(J - K)$ , where  $z$  is the coordination number [8, 33, 35, 36].

*Monte Carlo method with semiclassical  $SU(3)$  approximation.* We employ the semiclassical  $SU(3)$  approximation combined with classical Monte Carlo methods (s $SU(3)$ -MC) [31]. The wave functions are approximated by the direct product form of the one-body wave functions as

$$|\Psi\rangle = \bigotimes_{i=1}^N |\psi_i\rangle, \quad |\psi_i\rangle = \sum_{\alpha=x,y,z} d_{i,\alpha} |\alpha\rangle_i, \quad (2)$$

where  $d_{i,\alpha}$  is the complex coefficient satisfying  $|\mathbf{d}_i| = 1$ . The time-reversal invariant basis states  $|\alpha\rangle$  are given as

$$|x\rangle = \frac{i(|+1\rangle - |-1\rangle)}{\sqrt{2}}, \quad |y\rangle = \frac{|+1\rangle + |-1\rangle}{\sqrt{2}}, \quad |z\rangle = -i|0\rangle, \quad (3)$$

where  $|n\rangle$  ( $n = 0, \pm 1$ ) is the spin-1 state with  $S^z = n$ . The energy evaluated using this wave function,  $E_{\text{sSU}(3)} = \langle \Psi | \mathcal{H} | \Psi \rangle$ , is given as

$$E_{\text{sSU}(3)} = \sum_{\langle i,j \rangle} \left[ J |\mathbf{d}_i^* \cdot \mathbf{d}_j|^2 + (K - J) |\mathbf{d}_i \cdot \mathbf{d}_j|^2 \right] + ih \sum_{i=1}^N (\mathbf{d}_i^* \times \mathbf{d}_i)^z + \text{const.} \quad (4)$$

A set of parameters  $\{d_{i,\alpha}\}_{i=1,\dots,N}$  are updated by the standard classical MC sampling with the canonical ensemble of  $\exp(-\beta E_{\text{sSU}(3)})$ , where  $\beta = (k_B T)^{-1}$  is the inverse temperature. Spin moment whose  $z$ -component appears in the Zeeman term of Eq. (4) is given explicitly as

$$\mathbf{S}_i = \langle \psi_i | \hat{\mathbf{S}}_i | \psi_i \rangle = -i \begin{pmatrix} d_{i,y}^* d_{i,z} - d_{i,z}^* d_{i,y} \\ d_{i,z}^* d_{i,x} - d_{i,x}^* d_{i,z} \\ d_{i,x}^* d_{i,y} - d_{i,y}^* d_{i,x} \end{pmatrix}. \quad (5)$$

Spin quadrupolar operator,  $\hat{Q}_i^{\alpha\beta} = \hat{S}_i^\alpha \hat{S}_i^\beta + \hat{S}_i^\beta \hat{S}_i^\alpha - 2S(S+1)/3\delta_{\alpha\beta}$ , is a rank-2 traceless symmetric tensor, and its vector representation for five linearly independent components,  $\hat{\mathbf{Q}}_i = (\hat{Q}_i^{x^2-y^2}, \hat{Q}_i^{3z^2-r^2}, \hat{Q}_i^{xy}, \hat{Q}_i^{yz}, \hat{Q}_i^{zx})$ , is generally applied, which are evaluated as

$$\mathbf{Q}_i = \langle \psi_i | \hat{\mathbf{Q}}_i | \psi_i \rangle = \begin{pmatrix} -(|d_{i,x}|^2 - |d_{i,y}|^2) \\ -\frac{1}{\sqrt{3}} \left( 2|d_{i,z}|^2 - |d_{i,x}|^2 - |d_{i,y}|^2 \right) \\ - (d_{i,x}^* d_{i,y} + d_{i,y}^* d_{i,x}) \\ - (d_{i,y}^* d_{i,z} + d_{i,z}^* d_{i,y}) \\ - (d_{i,z}^* d_{i,x} + d_{i,x}^* d_{i,z}) \end{pmatrix}. \quad (6)$$

Our simulation is performed on the lattice of  $N = L \times L$ , with  $L = 12 - 36$  and  $L = 8 - 32$  for the triangular and

square lattices, respectively, under the periodic boundary condition. We combine the conventional Metropolis method with single spin rotations and replica exchange method [37], taking averages over the independent initial configurations using the jackknife resampling, each run consisting of  $10^6 - 10^7$  MC steps for thermalization and measurements, respectively.

The s $SU(3)$ -MC considers only the leading terms of the cumulant expansion of the partition function [31], which nevertheless incorporate enough amount of quantum and thermal fluctuations far beyond the simple mean-field calculation [38]. In fact, the description Eq. (2) is considered to describe well the nematic ground states of spin-1 BLBQ model on a triangular lattice [8, 33]. At finite temperature, the stochastic MC averages further allows us to include the spatial fluctuation effect intrinsic to the second order phase transition. In the same context, the s $SU(3)$ -MC has distinct advantages over the simple classical approximation which treats the spin moments as vectors [39]; in our case the vector  $\mathbf{d}_i$  represents the quantum quadrupole or the local quantum entanglement which orders by the BQ interaction, whereas the same interaction in classical method favors the collinear spin orderings [31].

An artifact of adopting the formally classical Hamiltonian Eq. (4) is the lack of quantum condensation at low temperature; the  $T^2$ -dependent specific heat characterizing the lowest energy excitations of three-colored Schwinger bosons of the spin-1 BLBQ model [8, 33, 40] is not observed [41]. However, in the temperature range at our focus, such behavior is easily wiped out by the thermal fluctuations and the collective behavior of quadrupoles become dominant, where the validity of Eq. (4) shall be recovered. In fact, the previous QMC calculations show that the specific heat deviates from  $T^2$  at  $T \sim T_c/2$  [29, 30].

*Ferroquadrupolar phase.* We first present the finite-temperature properties of the FQ states. Figure 1(a) shows the  $T$ - $h$  phase diagram for the triangular lattice at  $(J, K) = (0, -1)$  where the ground state has a FQ ordering. We determine the transition temperature  $T_c$  as the peak position of the specific heat  $C/N$ ; Figure 1(b) shows the temperature dependence of  $C/N$  in various magnetic fields. The peak position first slightly shifts to higher temperature and at  $h \gtrsim 1$  starts to move rapidly toward lower temperature. We compare the results of  $L = 12$  and  $36$  to show that the finite size effects are small enough, where  $T_c$  is always slightly lower and the peak-height increases for larger  $L$  for all values of  $h$  we examined. To understand this reentrant behavior of  $T_c$ , we analyze the  $T$ -dependence of the entropy density  $\tilde{s}(T, h)$  and the energy density  $e(T, h)$  in a weak field as shown in Figs. 1(c) and 1(d) [41];  $\tilde{s}(T, h)$  does not change much with  $h$  for the FQ phase. In contrast, the paramagnetic phase rapidly loses its entropy with  $h$  since the magnetic moment starts to align in the same direction. Since  $h$  gives a nearly constant shift in the energy  $e(T, h)$  common to both phases, which is dominated by the Zeeman

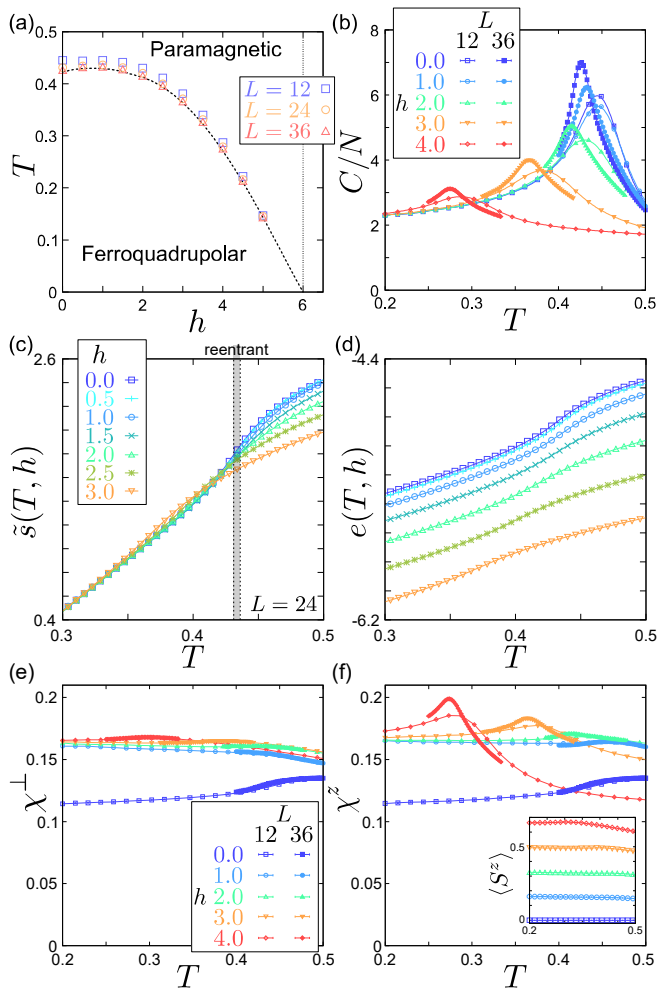


FIG. 1. Results of the sSU(3)-MC simulations on the triangular lattice at  $(J, K) = (0, -1)$ . (a)  $T$ - $h$  Phase diagram. Squares, circles, and triangles are the peak positions of the specific heat estimated by the Gaussian kernel approximation in  $L = 12, 24, 36$  samples, respectively. (b) Temperature dependence of the specific heat  $C/N$  for the various values of magnetic field  $h$  in  $L = 12$  (open) and 36 (filled) samples. (c), (d) Temperature dependence of the entropy  $\tilde{s}(T, h)$  and energy  $e(T, h)$  per site in  $L = 24$  sample. (e), (f) Temperature dependence of the magnetic susceptibilities perpendicular and parallel to the magnetic field for the various values of  $h$ , in  $L = 12$  (open) and 36 (filled) samples. The inset in (f) is the temperature dependence of the averaged magnetization density for  $L = 12$ .

term, the reentrant behavior is understood as an entropic effect.

Figures 1(e) and (f) show the magnetic susceptibilities of the spin component perpendicular and parallel to the magnetic field,  $\chi^\perp = (\chi^x + \chi^y)/2$ , and  $\chi^z$ , respectively, where  $\chi^\alpha = \beta N (\langle (S^\alpha)^2 \rangle - \langle S^\alpha \rangle^2)$ . One finds that  $\chi^z$  starts to develop a small peak at  $T_c$  when  $h$  is applied, indicating that the finite magnetic moment is induced along the  $z$ -axis. The value of  $\chi^\perp$  remains almost featureless, but a small structure appears at the

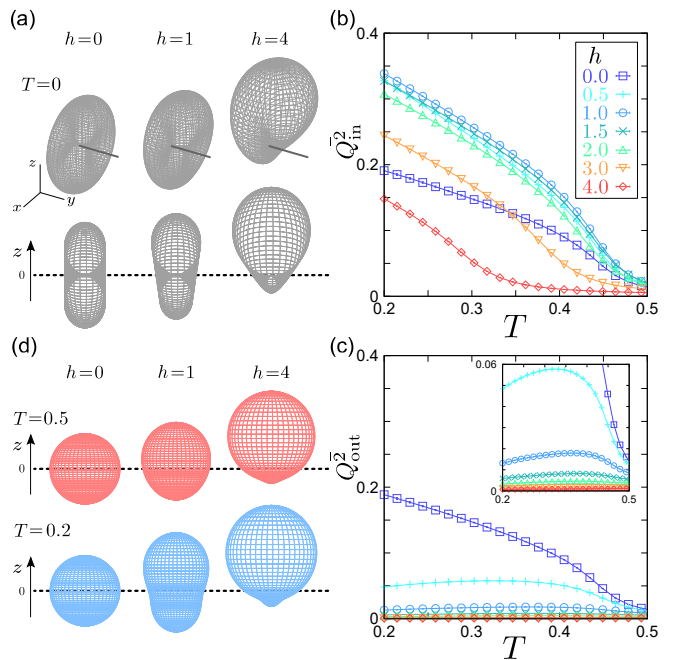


FIG. 2. (a) Spin-component distributions for the states at  $T = 0$  in a magnetic field where  $\mathbf{d} \in \mathbb{R}$  (bold line) is pointing in the  $y$ -direction. The lower panel is the view in the  $x$ -direction. (b), (c) Temperature dependence of (b)  $Q_{\text{in}}^2$  and (c)  $Q_{\text{out}}^2$  (Eq. (7)) in the  $L = 12$  triangular lattice. The inset in (c) is the enlarged view in the small  $Q_{\text{out}}^2$  region. (d) Spin-component distributions for the states evaluated by the sSU(3)-MC at  $T \neq 0$  and  $h = 0, 1, 4$  in  $L = 12$  triangular lattice, viewed perpendicular to the  $z$ -axis. The upper/lower panels belong to the paramagnetic/FQ phases. Since the calculation does not break the  $O(2)$  symmetry about the  $z$ -axis, the quadrupolar moments of  $T = 0.2$  ones are the averages of those of the symmetry broken ones with its director pointing in a particular direction, which is also consistent with the Mermin-Wagner theorem.

same position as  $\chi^z$  for larger  $L$ . The magnetization  $\langle S^z \rangle$  does not depend much on  $T$  and its value in the FQ phase is in good agreement with the ground state ones,  $m = h/[6(J - K)] = h/6$  (see inset of Fig. 1(f)) [8, 33].

We next examine the field-dependence of the quadrupolar moments. In the ground state, the magnetic field confines the  $\mathbf{d}$ -vector within the  $xy$ -space, namely,  $|\Psi\rangle = \bigotimes_{i=1}^N |\mathbf{d}_i\rangle$  with  $|\mathbf{d}_i\rangle = d_x |x\rangle + d_y |y\rangle$ . This is because  $h$  couples to  $d_x^* d_y - d_y^* d_x$  but not with  $d_z$  (see Eq. (4)). When  $\mathbf{d}$  is real, a pure quadrupole is formed  $O(2)$ -symmetric about the director  $\mathbf{d}$ , as shown in the first column of Fig. 2(a). At  $h \neq 0$  the emergent imaginary component of  $\mathbf{d}$  will distort it by shifting its fluctuation center toward the  $+z$ -direction [33] (see the second and third columns of Fig. 2(a)).

The relationship between  $\mathbf{d}$  and the shape of the quadrupole is understood more clearly from Eq. (6) as follows; when  $d_z$  is zero so do  $\langle Q^{yz} \rangle$  and  $\langle Q^{zx} \rangle$ , while  $\langle Q^{x^2 - y^2} \rangle$  and  $\langle Q^{xy} \rangle$  which consist only of  $x$  and  $y$  elements of  $\mathbf{d}$  can respond to  $h$ . Based on this consideration,

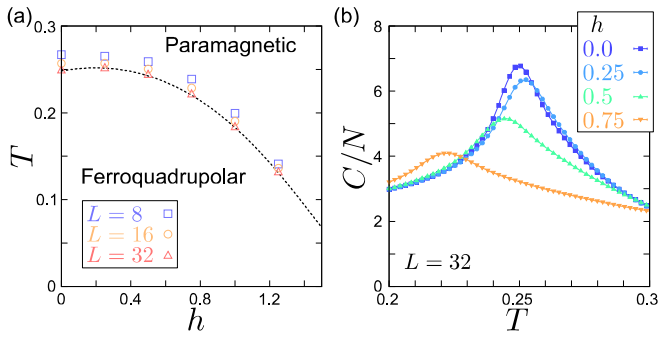


FIG. 3. (a)  $T$ - $h$  phase diagram and (b) the  $T$ -dependence of  $C/N$  for the square lattice at  $K/J = 2$  with  $J, K < 0$ .

we define two kinds of squared quadrupolar moments,

$$\begin{aligned} \bar{Q}_{\text{in}}^2 &= \frac{1}{2} \left( (Q^{x^2-y^2})^2 + (Q^{xy})^2 \right), \\ \bar{Q}_{\text{out}}^2 &= \frac{1}{2} \left( (Q^{yz})^2 + (Q^{zx})^2 \right), \end{aligned} \quad (7)$$

where we straightforwardly find  $\bar{Q}_{\text{in}}^2 \neq 0$  and  $\bar{Q}_{\text{out}}^2 = 0$  at  $T = 0$ .

Temperature dependences of  $\bar{Q}_{\text{in}}^2$  and  $\bar{Q}_{\text{out}}^2$  are shown in Figs. 2(b) and 2(c). In a weak field,  $\bar{Q}_{\text{in}}^2$  increases first and then at around  $h \gtrsim 1$  starts to decrease with  $h$ . Whereas,  $\bar{Q}_{\text{out}}^2$  takes a small but finite value at small  $h$  and  $T \neq 0$  because of the thermal fluctuation, and becomes  $\bar{Q}_{\text{out}}^2 = 0$  at  $T = 0$ . Notice that the apparently large values of  $\bar{Q}_{\text{out}}^2$  at  $h = 0$  simply because the moments are decoupled to the spatial coordinate. Once the field increases to  $h \gtrsim 1$ ,  $\bar{Q}_{\text{out}}^2$  is suppressed to zero for all temperatures. These results indicate that there is a crossover at  $h \sim 1$  from the low-field regime with a robust quadrupolar moment to the high field regime where the quadrupolar moment is rapidly suppressed with field. It apparently links with the reentrant behavior of  $T_c$  at  $h \lesssim 1$ . Such particular field-dependence of the quadrupolar moment is visualized in Fig. 2(d). Compared to the ones at  $T = 0$ , the quadrupoles at  $h = 1$  and  $T = 0.2$  has a gourd-shape which indicates that  $\mathbf{d}$  cants slightly off the  $xy$ -plane to maximize the fluctuation.

*Remarks.* The geometry of the lattice does not seem to play any intrinsic role. As shown in Figs. 3(a) and 3(b), we also perform the similar calculation for the square lattice at  $K/J = 2$  with  $J, K < 0$  [43], finding a reentrant behavior at  $h \lesssim 0.25$  [44].

In both Eqs. (1) and (4), the continuous symmetry exists, in which case a bulk finite-temperature phase transition is prohibited by the Mermin-Wagner theorem [45]. However, the specific heat shows a peak at  $T_c$  not only in our case but in the previous QMC calculations, which indicates the development of an intrinsic quasi-long range ordering [46]. The growth of correlation length at  $T_c$ , even if it does not diverge, will drive the system to a long range ordering once we stack the two-dimensional

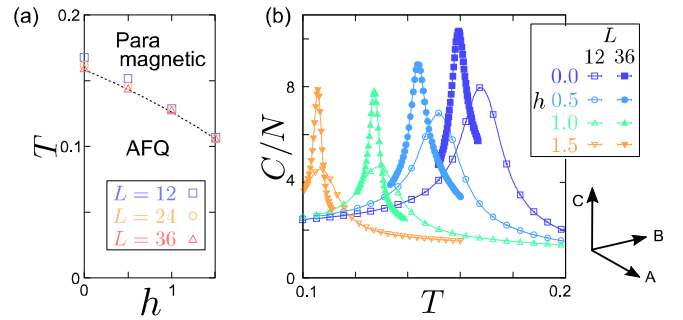


FIG. 4. (a)  $T$ - $h$  phase diagram and (b) the  $T$ -dependence of  $C/N$  for the triangular lattice with  $L = 12$  (open) and 36 (filled). The antiferroquadrupolar phase at  $K/J = 2$  with  $J, K > 0$  is studied [42], where A and B-sublattices gradually develop a magnetic moment similarly to that of the aforementioned FQ phase at  $T = 0$ . In the higher field range of  $h = 3/\sqrt{5} \approx 1.34$  to  $3(1 - 1/\sqrt{5}) \approx 1.658$  a  $2/3$  plateau phase appears, where the  $|\mathbf{d}_{i_C}\rangle = |z\rangle$  remains and the spins on A and B sublattices are fully polarized.

layer and include the inter-layer coupling, which is the situation expected for the actual material systems.

*Antiferroquadrupolar phase.* Finally, we briefly discuss the finite temperature properties and its field dependence for the antiferroquadrupolar (AFQ) phase. In the ground state of the triangular lattice, the AFQ is realized at  $0 < J < K$  [8–10]. The quadrupolar moments form a three-sublattice structure described by  $|\Psi\rangle = \bigotimes_{i=1}^{N/3} (|\mathbf{d}_{i_A}\rangle \otimes |\mathbf{d}_{i_B}\rangle \otimes |\mathbf{d}_{i_C}\rangle)$ , where  $i_\gamma$  ( $\gamma = A, B, C$ ) denotes the lattice sites with sublattice indices. At  $h \neq 0$  and  $T = 0$ , the spatial direction of  $\mathbf{d}_{i_\gamma}$  is fixed, and two of three components,  $|\mathbf{d}_{i_A}\rangle = |x\rangle$  and  $|\mathbf{d}_{i_B}\rangle = |y\rangle$ , behave similarly to the  $\mathbf{d}$ -vector of the FQ phase in a magnetic field, i.e.,  $d_x$  and  $d_y$  become complex numbers, while  $|\mathbf{d}_{i_C}\rangle = |z\rangle$  remains real [8]. Figure 4(a) shows the  $T$ - $h$  phase diagram;  $T_c$  decreases with increasing  $h$ , which can be detected clearly by the temperature dependence of the specific heat in Fig. 4(b) for the different values of  $h$  in  $L = 12$  and 36 samples. Although the quadrupoles on the A- and B-sublattices behave similar to that of the FQ phase, the difference lies in that they do not acquire a finite  $d_z$  and continue pointing within the  $xy$ -plane. In fact, the slight increase in  $T_c$  at small  $h$  is not observed in the case of AFQ. This is because the correlation between the quadrupoles of different sublattices do not allow the directors to cant off the original angle. The reentrant  $T_c$  is thus not observed for translational symmetry breaking AFQ ordering.

*Conclusion.* We disclosed the slight reentrant behavior of the paramagnetic-to-ferroquadrupolar spin nematic transition temperature in a weak magnetic field. Although both phases develop almost the same amount of magnetic moment by the field, only the nematic phase remains robust by modifying the shape of the quadrupolar moment toward the in-plane direction, and the counterpart paramagnet rapidly loses its entropy. One finds a common feature in  $^3\text{He}$  in that the entropies of solid and

liquid phases comes from the weakly interacting spin-1/2 nuclei and the condensed liquid of spins, respectively, although in their case the two phases are separated by the first order transition. If we regard the enthalpy  $+PV$  as our Zeeman term,  $-\langle S^z \rangle h$ , the Pomeranchuk effect, namely  $^3\text{He}$  is cooled by tracing the solid-to-liquid transition temperature in applying the pressure, would explain our increase of  $T_c$  with  $h$ . In both cases, the decrease of relative entropy per unit (volume or spin) of solid to liquid plays a crucial role to raise  $T_c$ . Similar field reentrant phase diagram is found in the uud plateau phase of the triangular lattice quantum magnet, where a large quantum fluctuation supported by the geometrical frustration

shall play a similar role to present quadrupolar fluctuation [47]. We thus conclude that the present phenomenon not only serves as a clue to explore elusive nematic phase, but adds to the list of universal entropic effect intrinsic to the physics of quantum liquid versus paramagnet.

*Acknowledgements.* We thank Hikomitsu Kikuchi, Yutaka Fujii, Karlo Penc, Katsuhiko Morita, and Tsutomu Momoi for fruitful discussions and comments. This work is supported by JSPS KAKENHI Grants No. JP17K05533, No. JP18H01173, No. JP17K05497, and No. JP17H02916. Part of the calculations is done using the facilities of the Supercomputer Center, Institute for Solid State Physics, University of Tokyo.

- 
- [1] J. Effantin, J. Rossat-Mignod, P. Burlet, H. Bartholin, S. Kunii, and T. Kasuya, *J. Mag. Mag. Mater.* **47-48**, 145 (1985).
- [2] T. Tayama, T. Sakakibara, K. Tenya, H. Amitsuka, and S. Kunii, *J. Phys. Soc. Jpn.* **66**, 2268 (1997).
- [3] W. Buyers, *Physica B* **223-224**, 9 (1996).
- [4] N. Shah, P. Chandra, P. Coleman, and J. A. Mydosh, *Phys. Rev. B* **61**, 564 (2000).
- [5] O. Suzuki, T. Goto, S. Nakamura, T. Matsumura, and S. Kunii, *J. Phys. Soc. Jpn.* **67**, 4243 (1998).
- [6] H.-H. Kuo, M. C. Shapiro, S. C. Riggs, and I. R. Fisher, *Phys. Rev. B* **88**, 085113 (2013).
- [7] A. F. Andreev and I. A. Grishchuk, *Sov. Phys. JETP* **60**, 267 (1984), [*Zh. Eksp. Teor. Fiz.* **87**, 467 (1984)].
- [8] A. Läuchli, F. Mila, and K. Penc, *Phys. Rev. Lett.* **97**, 087205 (2006).
- [9] H. Tsunetsugu and M. Arikawa, *J. Phys. Soc. Jpn.* **75**, 083701 (2006).
- [10] H. Tsunetsugu and M. Arikawa, *J. Phys.: Condens. Matter* **19**, 145248 (2007).
- [11] M. Sato, T. Momoi, and A. Furusaki, *Phys. Rev. B* **79**, 060406 (2009).
- [12] D. Podolsky and Y. B. Kim, *Phys. Rev. B* **79**, 140402 (2009).
- [13] M. Sato, T. Hikiyama, and T. Momoi, *Phys. Rev. B* **83**, 064405 (2011).
- [14] M. Sato, T. Hikiyama, and T. Momoi, *J. Phys.: Conf. Ser.* **320**, 012014 (2011).
- [15] R. Shindou, S. Yunoki, and T. Momoi, *Phys. Rev. B* **87**, 054429 (2013).
- [16] K. Nawa, M. Takigawa, M. Yoshida, and K. Yoshimura, *J. Phys. Soc. Jpn.* **82**, 094709 (2013).
- [17] A. Smerald and N. Shannon, *Phys. Rev. B* **88**, 184430 (2013).
- [18] O. A. Starykh and L. Balents, *Phys. Rev. B* **89**, 104407 (2014).
- [19] A. Smerald, H. T. Ueda, and N. Shannon, *Phys. Rev. B* **91**, 174402 (2015).
- [20] S. C. Furuya, *Phys. Rev. B* **95**, 014416 (2017).
- [21] A. Orlova, E. L. Green, J. M. Law, D. I. Gorbunov, G. Chanda, S. Krämer, M. Horvatić, R. K. Kremer, J. Wosnitza, and G. L. J. A. Rikken, *Phys. Rev. Lett.* **118**, 247201 (2017).
- [22] S. C. Furuya and T. Momoi, *Phys. Rev. B* **97**, 104411 (2018).
- [23] F. B. Ramos, S. Eliëns, and R. G. Pereira, *Phys. Rev. B* **98**, 094431 (2018).
- [24] B. Schmidt, P. Thalmeier, and N. Shannon, *Phys. Rev. B* **76**, 125113 (2007).
- [25] Y. Kohama, H. Ishikawa, A. Matsuo, K. Kindo, N. Shannon, and Z. Hiroi, *Proc. Natl. Acad. Sci. USA* **116**, 10686 (2019).
- [26] M. Skoulatos, F. Rucker, G. J. Nilsen, A. Bertin, E. Pomjakushina, J. Ollivier, A. Schneidewind, R. Georgii, O. Zaharko, L. Keller, C. Rüegg, C. Pfleiderer, B. Schmidt, N. Shannon, A. Kriele, A. Senyshyn, and A. Smerald, *Phys. Rev. B* **100**, 014405 (2019).
- [27] K. Harada and N. Kawashima, *J. Phys. Soc. Jpn.* **70**, 13 (2001).
- [28] K. Harada and N. Kawashima, *Phys. Rev. B* **65**, 052403 (2002).
- [29] R. K. Kaul, *Phys. Rev. B* **86**, 104411 (2012).
- [30] A. Völl and S. Wessel, *Phys. Rev. B* **91**, 165128 (2015).
- [31] E. M. Stoudenmire, S. Trebst, and L. Balents, *Phys. Rev. B* **79**, 214436 (2009).
- [32] I. Pomeranchuk, *Zh. Eksp. Teor. Fiz.* **20**, 919 (1950).
- [33] K. Penc and A. M. Läuchli, "Spin Nematic Phases in Quantum Spin Systems," in *Introduction to Frustrated Magnetism*, edited by C. Lacroix, P. Mendels, and F. Mila (Springer-Verlag Berlin Heidelberg, 2011) Chap. 13, p. 331.
- [34] T. A. Tóth, A. M. Läuchli, F. Mila, and K. Penc, *Phys. Rev. B* **85**, 140403 (2012).
- [35] B. A. Ivanov and A. K. Kolezhuk, *Phys. Rev. B* **68**, 052401 (2003).
- [36]  $z = 4, 6$  for the square and triangular lattices, respectively.
- [37] K. Hukushima and K. Nemoto, *J. Phys. Soc. Jpn.* **65**, 1604 (1996).
- [38] The simple mean-field approach assumes that  $\mathbf{d}_i$  in Eq. (2) is spatially uniform, whereas sSU(3)-MC allows  $\mathbf{d}_i$  to vary both in space and in Monte Carlo timescale, which takes account of the fluctuation other than and the quantum condensation effect referred in [41]. There, the fluctuation originating from the inter-site quantum entanglement can be replaced by the Monte Carlo averages. Particularly for the class of trivial long range order which are well approximated by the product state of the locally entangled unit (e.g., product of quadrupoles in Eq. (2)), the quantum and thermal fluctuation cannot

be discriminated, and the present treatment shall give a good description.

- [39] H. Kawamura and A. Yamamoto, *J. Phys. Soc. Jpn.* **76**, 073704 (2007).
- [40] S. Bhattacharjee, V. B. Shenoy, and T. Senthil, *Phys. Rev. B* **74**, 092406 (2006).
- [41] See Supplemental Material at [URL](#) for the details on the estimation of the low-temperature behavior and the entropy  $\tilde{s}(T, h)$ , which includes Refs. [48, 49].
- [42]  $J = 1/\sqrt{5}$  and  $K = 2/\sqrt{5}$ .
- [43]  $J = -1/\sqrt{5}$  and  $K = -2/\sqrt{5}$ .
- [44] See Supplemental Material at [URL](#) for the detailed results of the ferroquadrupolar phase in the square lattice.
- [45] N. D. Mermin and H. Wagner, *Phys. Rev. Lett.* **17**, 1307 (1966).
- [46] In the present study using the semiclassical approximation, the emergent quasi-long range order is related to the topological (Kosterlitz-Thouless) transition of binding-unbinding pairs of half-vortices [35]. The topological transition temperature generally falls slightly below the peak of the specific heat. However, it is not clear whether the fully quantum Hamiltonian Eq. (1) still shows such topological transition, since its possibility is excluded in the QMC study in Ref. [28] for the  $h = 0$  case on the square lattice.
- [47] H. Tsujii, C. R. Rotundu, T. Ono, H. Tanaka, B. Andracka, K. Ingersent, and Y. Takano, *Phys. Rev. B* **76**, 060406 (2007).
- [48] H. Kawamura, *J. Phys. Soc. Jpn.* **53**, 2452 (1984).
- [49] C. L. Henley, *Phys. Rev. Lett.* **62**, 2056 (1989).

# Supplemental Material for “Finite temperature thermodynamic properties of the spin-1 nematics in an applied magnetic field”

Katsuhiko Tanaka<sup>1</sup> and Chisa Hotta<sup>1</sup>

<sup>1</sup>*Department of Basic Science, University of Tokyo, Meguro, Tokyo 153-8902, Japan*

(Dated: September 16, 2020)

## I. LOW ENERGY PROPERTIES OF EQ. (4)

Here, the details of how we evaluated the entropy  $\tilde{s}(T, h)$  in the main text (Fig. 1(c)) is given.

Our sSU(3)-MC calculation is given for  $T \gtrsim 0.2$ . In order to evaluate the entropy from the specific heat, one needs to extrapolate these numerical results down to zero temperature. The nematic sSU(3) Hamiltonian Eq. (4) in the main text is formally a classical one that describes the interactions between the complex  $\mathbf{d}_i$ -vectors that represents the local one-body wave function. Similarly to the classical XY models (Refs. [48, 49]), its low-temperature behavior is evaluated by starting from the ground state and considering the low-energy harmonic branches.

The complex  $\mathbf{d}$ -vector on each site can be separated into the real and imaginary parts,  $\mathbf{d}_i = \mathbf{u}_i + i\mathbf{v}_i$ , where  $\mathbf{u}_i, \mathbf{v}_i \in \mathbb{R}$ .  $\mathbf{u}_i$  and  $\mathbf{v}_i$  satisfy the normalization condition,  $|\mathbf{u}_i|^2 + |\mathbf{v}_i|^2 = 1$ , and the overall phase can be fixed as  $\mathbf{u}_i \cdot \mathbf{v}_i = 0$  (Refs. [7, 33, 35]). For the ground state with both  $h = 0$  and  $h \neq 0$ , one can choose  $\mathbf{u}_i$  and  $\mathbf{v}_i$  to be  $\mathbf{u}_0$  and  $\mathbf{v}_0$ , whose values do not depend on  $i$  and are determined analytically (Refs. [8, 33, 34]). The lowest energy excitations are then obtained by varying these vectors as

$$\mathbf{u}_i = \mathbf{u}_0 + \delta\mathbf{u}_i, \quad \mathbf{v}_i = \mathbf{v}_0 + \delta\mathbf{v}_i. \quad (\text{S1})$$

For simplicity, we only consider the case where  $(J, K) = (0, -1)$  in the triangular lattice without a magnetic field, while we find shortly that the results do not depend on  $h$  or on the bilinear (Heisenberg) terms. The ground state has the ferroquadrupolar order, and  $\mathbf{u}_0$  and  $\mathbf{v}_0$  is chosen as

$$\mathbf{u}_0 = \begin{pmatrix} 1 \\ 0 \\ 0 \end{pmatrix}, \quad \mathbf{v}_0 = \mathbf{0}. \quad (\text{S2})$$

Then, the aforementioned local constraints on  $\mathbf{u}_i$  and  $\mathbf{v}_i$  are given as

$$2\delta u_i^x + (\delta\mathbf{u}_i)^2 + (\delta\mathbf{v}_i)^2 = 0, \quad (\text{normalization}) \quad (\text{S3})$$

$$\delta v_i^x + \delta\mathbf{u}_i \cdot \delta\mathbf{v}_i = 0. \quad (\text{overall phase fixing}) \quad (\text{S4})$$

The energy evaluated by the product state of the one-body wave functions can be rewritten up to  $O(\delta^2)$  as

$$\begin{aligned} E_{\text{sSU}(3)} &= - \sum_{\langle i,j \rangle} \left[ (\mathbf{u}_i \cdot \mathbf{u}_j - \mathbf{v}_i \cdot \mathbf{v}_j)^2 + (\mathbf{u}_i \cdot \mathbf{v}_j + \mathbf{v}_i \cdot \mathbf{u}_j)^2 + 1 \right] \\ &= -zN + \sum_{\langle i,j \rangle} \sum_{\alpha=y,z} \left[ \left( (\delta u_i^\alpha)^2 + (\delta v_i^\alpha)^2 \right) + \left( (\delta u_j^\alpha)^2 + (\delta v_j^\alpha)^2 \right) - 2(\delta u_i^\alpha \delta u_j^\alpha - \delta v_i^\alpha \delta v_j^\alpha) \right], \end{aligned} \quad (\text{S5})$$

Here, we drop the terms including  $\delta u_i^x$  and  $\delta v_i^x$  using the above constraints. These parameters are Fourier transformed as,

$$\delta\mathbf{u}_\mathbf{k} = \frac{1}{\sqrt{N}} \sum_{i=1}^N e^{-i\mathbf{k} \cdot \mathbf{r}_i} \delta\mathbf{u}_i, \quad \delta\mathbf{v}_\mathbf{k} = \frac{1}{\sqrt{N}} \sum_{i=1}^N e^{-i\mathbf{k} \cdot \mathbf{r}_i} \delta\mathbf{v}_i, \quad (\text{S6})$$

and the energy  $E_{\text{sSU}(3)}$  can be diagonalized as

$$E_{\text{sSU}(3)} = E_0 + \sum_{\mathbf{k}} E_{\mathbf{k}}, \quad (\text{S7})$$

where

$$E_0 = -zN, \quad (\text{S8})$$

$$E_{\mathbf{k}} = \sum_{\alpha=y,z} [(-\gamma_{\mathbf{k}} + z) \delta u_{\mathbf{k}}^{\alpha} \delta u_{-\mathbf{k}}^{\alpha} + (\gamma_{\mathbf{k}} + z) \delta v_{\mathbf{k}}^{\alpha} \delta v_{-\mathbf{k}}^{\alpha}], \quad (\text{S9})$$

$$\gamma_{\mathbf{k}} = 2 \left[ \cos k_x + \cos \left( \frac{k_x + \sqrt{3}k_y}{2} \right) + \cos \left( \frac{k_x - \sqrt{3}k_y}{2} \right) \right]. \quad (\text{S10})$$

Performing the Gaussian integral, the partition function is calculated as

$$Z \simeq \int e^{-\beta E_{\text{sSU}(3)}} \prod_{\mathbf{k}} d(\delta u_{\mathbf{k}}^y) d(\delta u_{\mathbf{k}}^z) d(\delta v_{\mathbf{k}}^y) d(\delta v_{\mathbf{k}}^z) \simeq e^{-\beta E_0} \prod_{\mathbf{k}} \left[ \frac{\pi^2}{\beta^2} (\det \mathcal{E}_{\mathbf{k}})^{-\frac{1}{2}} \right], \quad (\text{S11})$$

where

$$\det \mathcal{E}_{\mathbf{k}} = \begin{pmatrix} -\gamma_{\mathbf{k}} + z & & & \\ & -\gamma_{\mathbf{k}} + z & & \\ & & \gamma_{\mathbf{k}} + z & \\ & & & \gamma_{\mathbf{k}} + z \end{pmatrix}. \quad (\text{S12})$$

Then, the statistical average of the energy density,  $e(T, h = 0)$ , is

$$e(T, h = 0) = \frac{1}{N} \left( -\frac{\partial}{\partial \beta} \ln Z \right) = \frac{E_0}{N} + 2k_{\text{B}}T, \quad (\text{S13})$$

and the specific heat in the low-temperature region,  $c(T, h = 0)$ , is

$$c(T, h = 0) = \frac{\partial e(T, h = 0)}{\partial T} = 2k_{\text{B}}. \quad (\text{S14})$$

So far, we assumed the particular case  $h = 0$  and  $J = 0$  with a ferroquadrupolar ground state. However, since this result is nothing but a law of equipartition of energy, the number of low energy modes are responsible, and the same conclusion on  $e(T, h)$  and  $c(T, h)$  holds even for  $h \neq 0$  and  $J \neq 0$  as far as the ground state remains ordered, and only the detailed form of  $E_0$  and  $E_{\mathbf{k}}$  is modified. The geometry of the lattice, namely the square lattice, also does not change the result as far as it is in two dimension.

Based on the above consideration, one can assume the temperature dependence of the energy in the low-temperature region as

$$e(T, h) = e(0, h) + 2k_{\text{B}}T + \alpha(h)T^{\gamma(h)}, \quad (\text{S15})$$

where  $e(0, h)$  is the exact ground states energy of  $E_{\text{sSU}(3)}$  given in Refs. [8, 33, 34], and  $\alpha(h)T^{\gamma(h)}$  with  $\gamma(h) > 1$  is the correction beyond  $O(\delta^2)$  from Eq. (S13). The actual values of  $\alpha(h)$  and  $\gamma(h)$  are evaluated by fitting the calculated data. Fitted data is shown in Fig. S1 for  $L = 24$  triangular lattice. Then, the specific heat is calculated as

$$c(T, h) = \frac{\partial e(T, h)}{\partial T} = 2k_{\text{B}} + \alpha(h)\gamma(h)T^{\gamma(h)-1}, \quad (\text{S16})$$

and the entropy density is given as

$$s(T, h) = \int_0^T \frac{c(T', h)}{T'} dT' = \int_0^T \frac{2k_{\text{B}}}{T'} dT' + \frac{\gamma(h)\alpha(h)}{\gamma(h) - 1} T^{\gamma(h)-1}. \quad (\text{S17})$$

The divergent first term  $\int_0^T \frac{2k_{\text{B}}}{T'} dT'$  is the artifact of dealing with the low energy branches classically. In fact, the original spin-1 BLBQ Hamiltonian (Eq. (1) in the main text) is known to exhibit  $T^2$ -dependent specific heat at lowest temperature range, which originates from the excitation of three-colored Schwinger bosons (Refs. [8, 33, 40]). This kind of quantum condensation effect is dropped off in  $E_{\text{sSU}(3)}$ , and instead a classical divergent term appears as an artifact. However, since this term contributes to all cases as common constant shift where the above discussion holds regardless of the values of  $h$  and  $J$ , which no longer plays an important role in discussing the higher temperature range at our focus. We thus drop this term and deal with  $\tilde{s}(T, h) = s(T, h) - \int_0^T \frac{2k_{\text{B}}}{T'} dT'$  in the main text.

We show  $e(T, h)$  and  $\tilde{s}(T, h)$  obtained by the same treatment for the square lattice in Fig. S2.

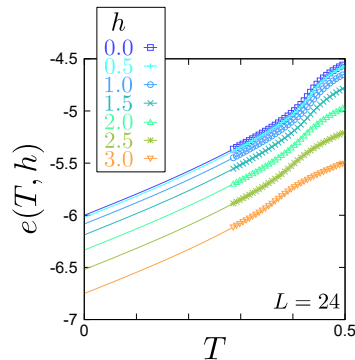


FIG. S1. Energies in the various magnitude of magnetic field in the  $L = 24$  triangular lattice with  $(J, K) = (0, 1)$ . Symbols denote the data obtained by the sSU(3)-MC simulations, and the lines are the energy estimated by fitting the sSU(3)-MC data.

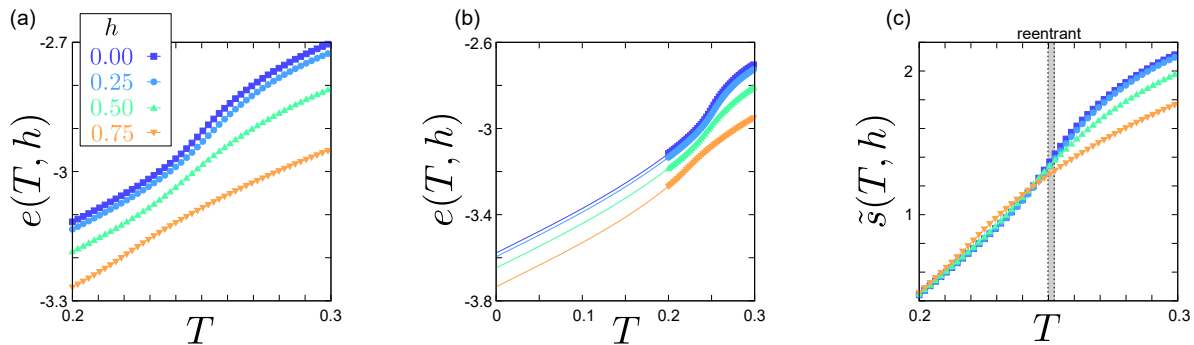


FIG. S2. The evaluated energy and entropy for the  $L = 32$  square lattice. The parameters are set as  $K/J = 2$  with  $J^2 + K^2 = 1$  and  $J, K < 0$ , i.e.,  $(J, K) = (-1/\sqrt{5}, -2/\sqrt{5})$ . (a)  $e(T, h)$  around the phase transition temperature. (b)  $e(T, h)$  in the wider temperature region. Lines in the low-temperature region is the energy estimated from the sSU(3)-MC results. (c) Entropy  $\tilde{s}(T, h)$  estimated by the above procedure.

## II. DETAILS ON THE FINITE-TEMPERATURE PROPERTIES OF THE FERROQUADRUPOLAR PHASE IN THE SQUARE LATTICE

We show the detailed results of the semiclassical SU(3) Monte Carlo (sSU(3)-MC) simulation (Ref. [31]) for the ferroquadrupolar phase in the square lattice with  $L = 32$  (Fig. S3). The parameters are set as  $K/J = 2$  with  $J, K < 0$ , i.e.,  $(J, K) = (-1/\sqrt{5}, -2/\sqrt{5})$ , where the variational ground state is the ferroquadrupolar phase in the absence of the magnetic field (Refs. [33, 34]).  $T$ - $h$  phase diagram and the temperature dependence of the specific heat are given in Figs. 1(c) and 1(d) in the main text.

Figures S3(a) and (b) show the temperature dependence of the magnetic susceptibilities of the perpendicular and parallel components of spins to the external magnetic field applied along  $z$ -axis, respectively. The inset in Fig. S3(b) is the averaged magnetization density. Figures S3(c) and (d) are the temperature dependence of  $Q_{\text{in}}^2$  and  $Q_{\text{out}}^2$ , respectively. The expressions of  $Q_{\text{in}}^2$  and  $Q_{\text{out}}^2$  are given in Eq. (7) in the main text. We emphasize here that all of these results are qualitatively similar to the ones in the triangular lattice discussed in the main text, which indicates that these behaviors are inherent to the ferroquadrupolar phase and independent of the lattice geometry.

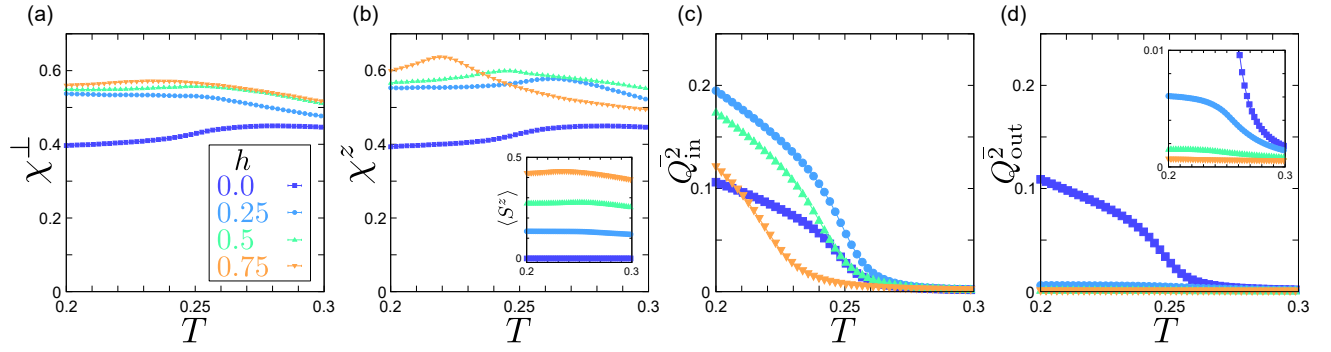


FIG. S3. Detailed results of the sSU(3)-MC simulation for the ferroquadrupolar phase in  $L = 32$  square lattice. The parameters are set as  $K/J = 2$  and  $J, K < 0$ , i.e.,  $(J, K) = (-1/\sqrt{5}, -2/\sqrt{5})$ . (a), (b) Temperature dependence of the magnetic susceptibilities (a) perpendicular and (b) parallel to the magnetic field for the various values of  $h$ . The inset in (b) is the temperature dependence of the averaged magnetization density  $\langle S^z \rangle$ . (c), (d) Temperature dependence of (c)  $Q_{\text{in}}^2$  and (d)  $Q_{\text{out}}^2$  (Eq. (7) in the main text). The inset in (d) shows the enlarged view in the small  $Q_{\text{out}}^2$  region.